Preliminary Results of an Upgraded Atmospheric Visibility Monitoring Station

B. Sanii,[1] A. Datta,[1] D. Tsiang,[2] J. Wu,[1] and A. Biswas[1]

The Atmospheric Visibility Monitoring (AVM) station located at the Table Mountain Facility (TMF) in Wrightwood, California, recently has undergone a significant hardware and software upgrade. This upgrade has enhanced our ability to pursue the AVM program goals, which are to gather atmospheric optical transmission data at specific wavelengths and to build statistical attenuation models for space-to-ground optical communication links. The AVM stations derive information about atmospheric transmission by continuously monitoring and recording star intensities. The TMF AVM has been operational since October 1999, and enough data have been accumulated to provide a first glimpse into the capabilities of the new system. In doing so, problems were identified in the star identification software routines implemented as a part of the on-site image processing, and new processing routines have been developed. By post-processing of stored images, the procedure has resulted in a 33 percent increase in viable star images. The upgraded system continues to prove to be more convenient to maintain and holds the promise of significant improvements in the quality and quantity of the usable data.

I. Introduction and Background

Successful space-to-Earth optical communications system design requires a good understanding of signal loss due to the Earth's atmosphere. The atmosphere attenuates the optical signal as light is absorbed and scattered by particles in its path down to the ground receiving station. Losses in distortions of the optical signal also result from atmospheric turbulence; however, this is discussed elsewhere [1], and this article will be dedicated to attenuation only. Atmospheric attenuation must be properly budgeted when performing optical communication link analysis in order to provide adequate margin. Unlike radio-frequency communication, cloud and precipitation result in a complete link loss of the optical channel. Thus, reliable statistics of channel availability are needed to assess overall link availability. The goal of the Atmospheric Visibility Monitoring (AVM) program [2–4] is to gather data over an extended period so that reliable statistics can be compiled. Moreover, by gathering data from diverse sites and convolving their

[1] Communications Systems and Research Section.

[2] Tracking Systems and Applications Section.

The research described in this publication was carried out by the Jet Propulsion Laboratory, California Institute of Technology, under a contract with the National Aeronautics and Space Administration.

statistical availability, it is expected that the optical channel availability can be significantly enhanced [4].[3] Thus, the high data rates and site diversity are expected to provide an augmentation in data downlink capacity required for future NASA missions [5].

The AVM program is operated by the Optical Communications Group (OCG) at JPL. Data gathered and processed are used to build statistical models of atmospheric transmission at optical frequencies ranging from the visible to the near infrared. It is expected that these data also will provide guidance in site selection of ground receiving stations.

The program consists of three autonomous observatories and a database of atmospheric transmission data taken from the observatories. Each of the three observatories is stationed in the southwestern United States. The three sites are located at Mt. Lemmon (near Tucson, Arizona), the Table Mountain Facility (TMF, near Wrightwood, California), and Goldstone (near Barstow, California). The Goldstone AVM was transplanted there from the Mesa site (near JPL), where it originally was assembled for prototype testing. Currently, the Table Mountain and Mt. Lemmon AVMs have been upgraded and are now gathering and processing data using new cameras, computers, and control software. The third (and oldest) AVM, at Goldstone, currently is undergoing repairs.

Using site-calibrated telescopes, the observatories take photometric readings of non-variable, brighter than magnitude-four stars through six optical filters. Three of these filters pass thin bandwidths of light that correspond to laser wavelengths that may be used in future free-space optical communications systems, including 532 nm (frequency-doubled Nd:YAG), 1064 nm (an Nd:YAG laser), and 860 nm (a common diode laser). In addition to these, there are three other broadband astronomical filters (the standard visual, infrared, and red filters), though there are plans (discussed below) to experiment with replacing them with filters that will enable us to measure sky background light as a function of polarization.

Photometric measurements of stars are obtained as a function of elevation angle by having the observing telescope perform autonomous sidereal tracking. These measurements are used to estimate the starlight's spectral intensity incident above the atmosphere. These estimated intensities serve as calibration constants for a given star, filter, and telescope combination. Using the calibration constants, attenuation values are assigned to intensities obtained from images of stars. Attenuation data obtained in this manner then can be represented in cumulative distribution function plots (CDFs). These plots provide the statistical basis for predicting availability and attenuation for future optical communication links. The three site computers are network synchronized to a common and reliable clock (the Massachusetts Institute of Technology gateway to the atomic clock) periodically and automatically, in order to follow a truly identical 15-minute cycle. Consequently, the same stars are being observed at the same time at the three sites, allowing for site-diversity analysis.

In July of 1999, the Table Mountain AVM was upgraded with a new camera, computer, and control software.[4] The new system enabled considerably improved daylight observation and 1064-nm wavelength measurements, as well as more in-line data reduction. This resulted from the new charge-coupled device (CCD) camera being thermoelectrically cooled and having much lower dark noise so that the long exposures required to obtain star images, even in the daytime, can be made. Furthermore, the new systems are networked and are remotely accessible for monitoring and control from JPL. This automatically has resulted in shorter station outage times. A summary of the significant upgrade characteristics is contained in Table 1. Figure 1 illustrates the relative increase, in percentage format, of good star images gathered with the new system. Figure 2 shows a representative star image acquired with the new camera system.

[3] K. Shaik and M. Wilhelm, "Ground Based Advanced Technology Study (GBATS)," JPL D-11000, Release 1 (internal document), Jet Propulsion Laboratory, Pasadena, California, August 1994.

[4] C. Edwards, "NASA's Deep Space Telecommunications Roadmap," viewgraph presentation (internal document), Jet Propulsion Laboratory, Pasadena, California, January 22, 1998.

Using several months of dependable data gathered at TMF, a statistical analysis has been performed to assess and validate the system's performance.

Table 1. Original and updated AVM system characteristics.

Computer		
Original hardware/software	Upgraded hardware/software	Benefit
DOS based	Windows NT based	More recent software may be employed
Written in Borland Turbo C++ (in 1994)	Written in Microsoft Visual C++ Version 6.0	Enables Windows-based interface
Turbovision-based user's interface (no longer supported)	Windows user's interface	Greater ease of use
Program functions are written into main program as needed (many times over and over)	Functions are written in modules once (main program calls on function modules as needed)	Easier to determine which portion of the code may need modification
Not network compatible	Network compatible	Much maintenance may be performed from JPL
Data processing performed at JPL requiring many MB of data transferred daily from each site	First-order data processing performed in real time at each site	Less time is lost transferring data
System variables are hard coded into complied code	System site and alignment variables are changed in user interface	Program does not need to be recompiled at the site when modifications are needed
Not year 2000 compatible	Year 2000 compatible	No dating issues
Star image can be seen only at site computer	Star image can be viewed at site and remote computers	Easier site verification and troubleshooting
Star position data requires annual update	Star position is adjusted for current epoch from published year 2000 data	Less intervention required
Not compatible with new CCD camera	Compatible with new CCD camera	See below
Camera		
Original CCD	Upgraded CCD	Benefit
Spectra Source Lynxx PC plus	Apogee AP7	—
165×192 pixels	500×500 pixels	—
3.8×3.3 arcsec FOV per pixel	1.9×1.9 arcsec FOV per pixel	Greater angular resolution per pixel
10.5×10.5 arcmin FOV for imager	15.8×15.8 arcmin FOV for imager	—
−6 db readout noise	−38 db readout noise	Less noise (allows daytime and long exposures)
12-bit resolution	16-bit resolution	Greater intensity resolution
1064-nm quantum efficiency <1.5%	1064-nm quantum efficiency = 8%	Better images at 1064 nm
Typical exposure time for 1064-nm measurement >5 min	Typical exposure time for 1064-nm measurement = 1 min	15-min cycle time may be adhered to

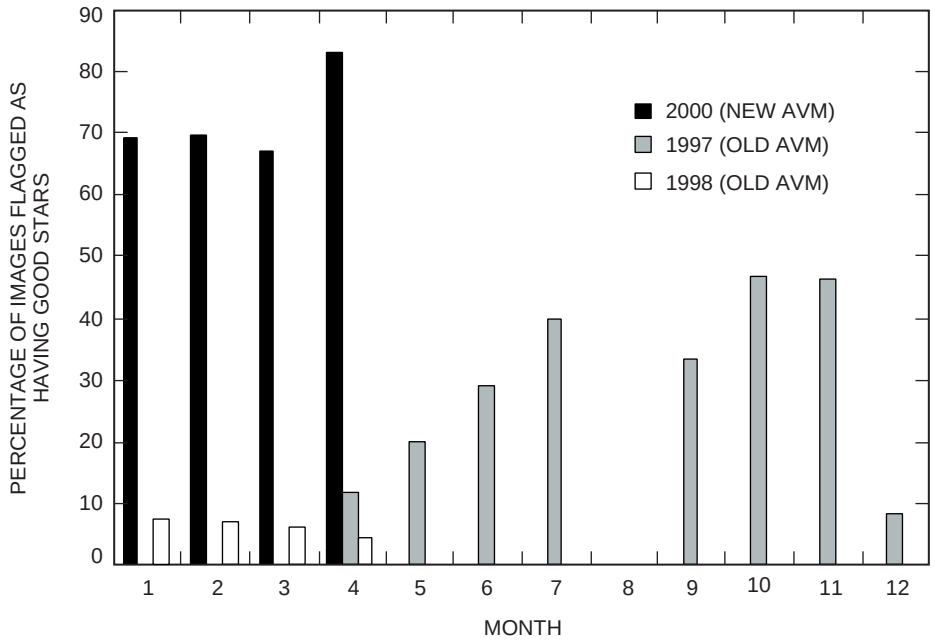

Fig. 1. Comparison of AVM images taken with the old and new cameras. The new camera shows a marked improvement in the percentage of images containing a visible star. These percentages are an indication of how often a star can be seen, day or night, in the absence of observing conditions that induce roof closure. 1997 and 1998 percentages are shown for comparison over the length of the year. A better comparison may be drawn as more data become available.

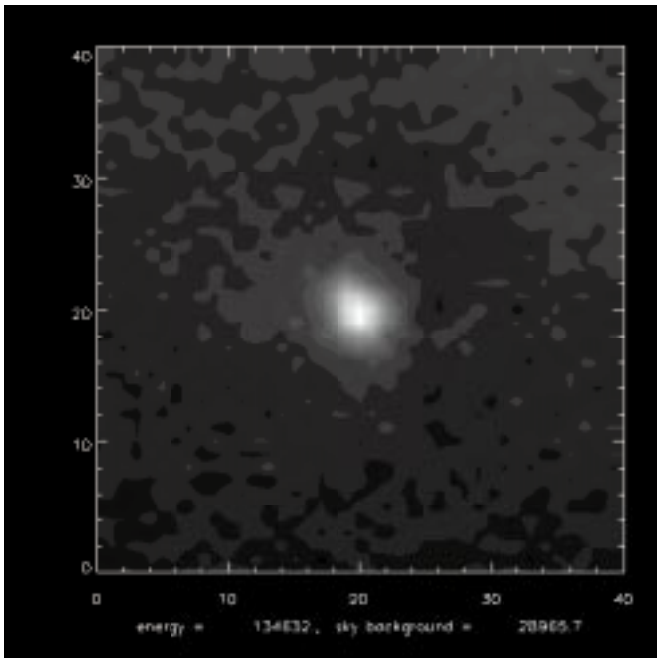

Fig. 2. A sample daytime image of star Beta Gemini gathered through the 1064-nm filter. The exposure time required to acquire this image was 15 s.

II. Analysis

The best basis for validation of the AVM lies in the results of the star-calibration routines. These routines are performed with data gathered over a specific duration. The reliability of the cumulative distribution function is highly sensitive to the calculated calibration values.

The AVM program is primarily interested in the transmission of the star's light through the atmosphere, and details such as different star spectral intensities, camera sensitivity, and telescope optics need to be calibrated out. Originally, much of this was intended to be done by way of a known illumination source in the AVM and the previously studied camera sensitivities and star spectral intensities. However, keeping the illumination source constant over time proved to be cumbersome, especially for the desired autonomous mode of operations.

A calibration procedure to determine the intensity of a given star incident on the Earth's atmosphere in AVM units (meaning the arbitrary units corresponding to camera pixel values after passing through the AVM optics) thus was devised. This procedure is based on the fact that the average atmospheric attenuation is a function of the elevation angle above the horizon, or (in a more analytically tangible form) it is an exponential function of air mass that the star's light must pass through [6]. Thus, by looking at the maximum detected star intensity for various air masses (a function of the known elevation angle), one may logarithmically plot a curve that can be linearly fit to the exponential function. This fit will allow us to extrapolate to the expected intensity of the star light that has passed through an air mass of zero (i.e., above the atmosphere). This intensity is also, by definition, in AVM units.

The procedure relies on certain assumptions. Atmospheric attenuation of star light arises due to molecular absorption, molecular or Raleigh scattering, and particulate scattering. Deviations from the exponential relation between intensity and air mass due to, for example, collision-induced spectral absorption line broadening [7] and multiple particulate scattering [7,8] have been cited in the literature. In this preliminary work, however, these effects are ignored, and a more detailed evaluation will be performed in the future. It also is assumed that the intervening medium between the star and Earth stays relatively constant in the relatively short time interval of our lifetimes.

As mentioned, the calibration constants influence the CDFs, and a reliable approach to determining calibration constants is needed. Alternate strategies are available in sampling data used for calibration. One approach is to select the maximum star intensities corresponding to a given air mass over an extended period of observation. However, this assumes that the telescope and filter transmission remain constant over extended periods. A second approach is to acquire calibration data on selective nights that offer ideal observing conditions. This is cumbersome and requires either predicting an ideal observing night in advance or identifying one by sorting through the data, and it has not been tried yet. Finally, a third approach would be to monitor the correlation constant between the data and the predicted fit and select a subset of data that provides the best correlation. The third approach needs monitoring of the calibration constants over an extended period of time. The rationale for the third approach is that the initial few weeks may not provide sufficient data to provide representative fits of intensity versus air mass, while taking data from too long a period will introduce errors due to seasonal variations in the observing system.

Of course, a very important consideration in selecting calibration data is to ensure that the brightest pixels of overhead clouds or other artifacts, such as camera noise, are not mistaken for stars. This brings up the issue of "flagging," where each image is assigned a number that corresponds to the confidence in its quality and its likelihood of containing a star. The flagging is an issue of image-analysis software. The original version of the upgraded software was not flagging in a consistent and believable manner. The old method flagged based upon the metrics of maximum pixel divided by background, maximum pixel distance from the center of the field of view, and star intensity divided by background. While the metrics are reasonable, their implementation was questionable, and their results were visibly incorrect. By the time this was properly diagnosed, much data had been accumulated. Consequently, an improved

re-flagging program was written in MatLab. This program reads in the reduced images that the AVM saves and produces an output file with the newly recorded flags, while storing the old flag in an unused field. Figure 3 demonstrates how the new flagging routines are individually more effective than the old ones, and Fig. 4 illustrates the magnitude of changes that this flagging routine had to make. All in all, 34 percent of the images were incorrectly flagged and mistakenly labeled as not containing star images, whereas the new flagging routine clearly and reliably rectified this problem. In Fig. 3, one can see a square of asterisks in each image (except the bottom right, where the nature of the CCD error is interpreted as negative intensity). This is the smallest square in the image that contains 80 percent of the total intensity, after the background has been subtracted. The background is defined as the average pixel value of the perimeter of the image. Various other marked points in the image include the average location of the greatest gradient in the image from four directions ($\bigtriangledown$), the brightest pixel ($\bullet$), the brightest 3-by-3 pixel box (*), and the center of the box containing 80 percent of the image energy ($\times$). If all these points are within the 80 percent box and the signal-to-noise ratio (SNR) is above a threshold (SNR is defined as the ratio of the pixel value in the 3-by-3 box over the background after compensating for exposure time), then the star gets the flag of four. A flag of four is interpreted by the post-processing data analysis system (an array of Microsoft Access tools and reports) as a viable candidate for calibration. A flag of

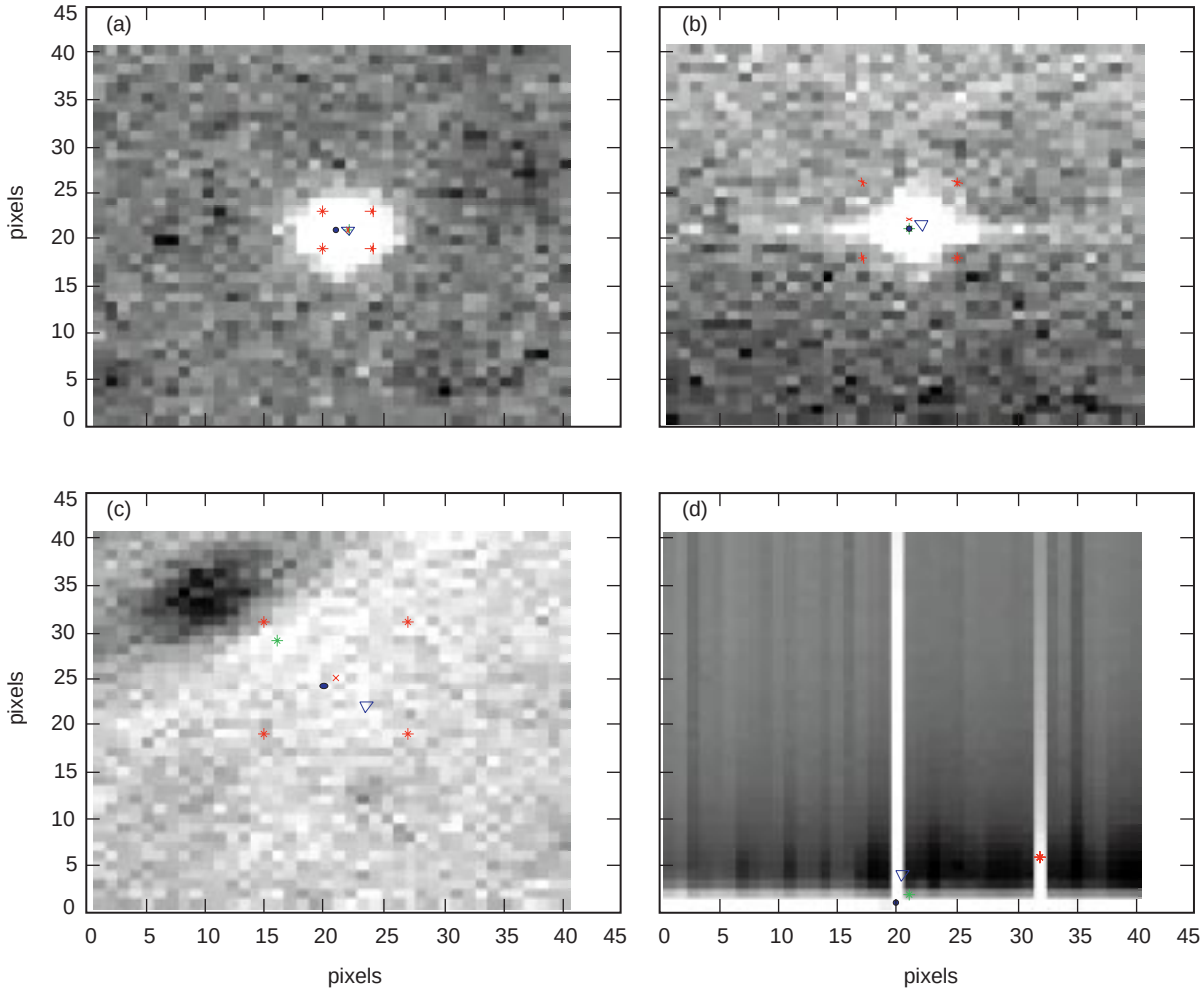

Fig. 3. AVM images illustrating star flagging: (a) and (b) were previously flagged as having no star, but were caught as good candidates for calibration by the new flagging routines, and (c) and (d) were previously flagged as good stars for calibration, but were correctly identified by the new flagging routine as being poor star candidates. (Figure 3(d) is probably the result of a CCD readout error.)

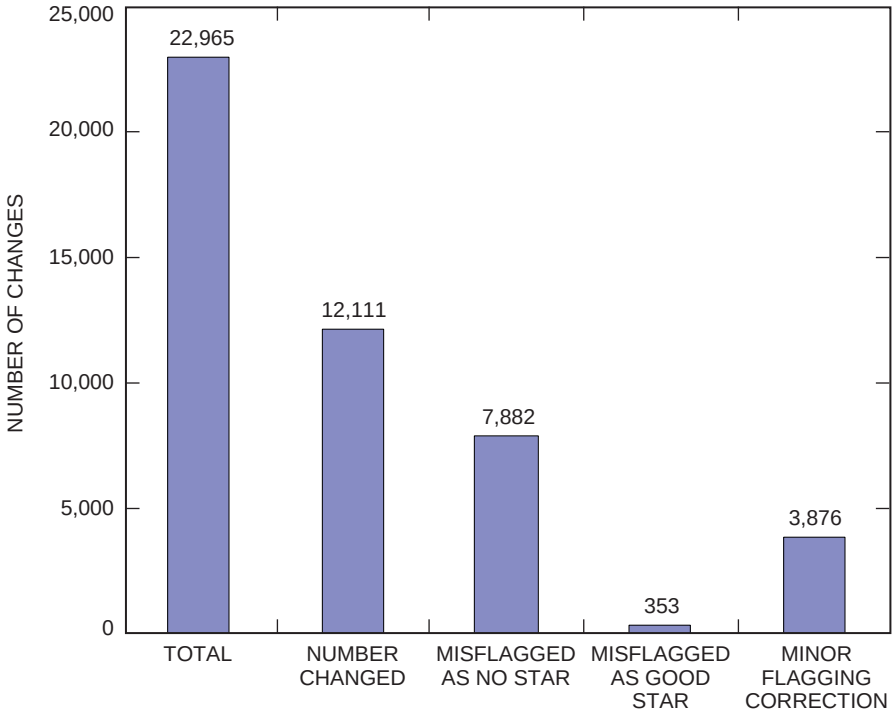

Fig. 4. Reflagging performed by the new process from January to March 2000. A minor flagging correction is defined as being between flag two and one (bad and worse; flag two is no longer used in the new flagging scheme) or between three and four (good and excellent). As seen, the majority of the misflagging is of stars that should be designated as good but which were designated as poor.

three indicates that there may indeed be a star there, however its intensity is weak, making it unsuitable for calibration. A flag of one indicates that there is very little likelihood of having a star in the image (flag two is no longer in the new flagging scheme). Flagging is very important because the book-keeping of the Access report for cumulative distribution functions automatically logs flag-one stars as having an extremely large attenuation that approximates opacity.

Incorrect flagging of the stars results in many post-processing misinterpretations. The routines are not as rigorous as they could be, because the AVM still is limited by processing power; an overly involved flagging routine would slow down the observation cycle such that fewer data would be acquired. If the cycle exceeds the 15-minute window it is currently set to, the next cycle will be missed. Consequently, consistent over processing would result in half available data, unless the window size were changed. A bound has not yet been set on the required processing power for a thorough analysis, and changing the window size currently is not being pursued. This MatLab program process was written with the intention of replacing the current flawed flagging software that is part of the on-site data reduction. The process flow of the flagging routine to be implemented as a part of the on-site image processing is provided in the Appendix.

Another issue that has been uncovered in the preliminary analysis is CCD half-well overflow. To protect against the saturation of the CCD camera (which would skew the star-energy value), the camera determines its correct exposure time by performing a half-well, that is, exposing the CCD until the brightest group of pixels is at the middle of its possible range of values. If a situation were to arise where the star was completely blocked when this process was occurring, the exposure time would be limited by the electrical noise level of the cooled CCD, resulting in an extremely long exposure. This time loss also would slow down the observation cycle of the AVM, and so it is wisely limited by preset values. However,

it was discovered that when the half-well dictated an exposure greater than the limit, the system would default to a prescribed, extremely brief exposure. This image is not suitable for calibration purposes because it does not take advantage of the CCD's available dynamic range and is likely to be washed out as noise. Images taken with the 1064-nm filter are particularly susceptible to this, because the spectral sensitivity reduction of the CCD would mandate longer exposures. The extremely brief exposure that results from incorrect half-welling can be interpreted by the program as dense cloud cover instead of just a dim star. This introduces a false bias in the data, and, consequently, the Microsoft Access post-processing routine has been modified to exclude images that suffer from half-well overflow.

Now that one may feel more confident in the validity of the star images used for calibration purposes, one may compare the calibration values of the upgraded AVM system from month to month for consistency. Furthermore, one may compare some of the values (the ones that are independent of the CCD imager) with the previous AVM system. A sample calibration plot is shown in Fig. 5, which plots the brightest-flag four-star images passing through different air masses. From the slope and intercept of this plot, we may gather the intensity of the star incident on the atmosphere and the per-air-mass attenuation of the atmosphere under ideal conditions. The mean absolute deviation of the star values with the fitted straight line also is recorded. Based on these values, the optimal set of calibration constants at 860 and 532 nm were determined to be those using star images from January through February 2000. However, for 1064 nm, the absolute deviation remained nearly flat over the period from January to April 2000. Monitoring of these deviations needs to be carried out over longer periods in order to identify trends or variations with certainty. For the present data, we have chosen calibration constants that offered the least absolute deviation.

A cumulative distribution function (CDF) is presented in Fig. 6. As in CDFs produced with the old AVM setup, the 860-nm and 1064-nm wavelengths have a better statistical transmission than does the 532-nm wavelength. One measure of the performance of a wavelength and site is the 3-dB point, where attenuation is about half. This plot indicates that the 3-dB point for Table Mountain from January to April 2000 is 81 percent for 532 nm, 79 percent for 860 nm, and 75 percent for 1064 nm. This may be interpreted to indicate that 1064 nm is not a very good window for communication links, but other more likely effects are present. Specifically, because the camera's response at 1064 nm is so much worse than at 860 nm (8 percent quantum efficiency versus 70 percent at 860 nm), sometimes the star is not detectable by the camera within allowable exposure times and is logged as cloud cover. Calibration corrections cannot correct

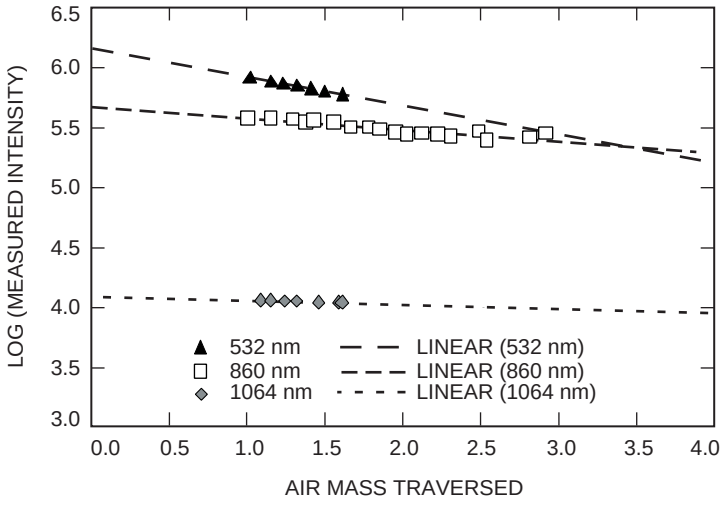

Fig. 5. A sample calibration plot, used to determine the pre-atmosphere star intensity in AVM units, which is used as a basis of determining the attenuation through the atmosphere.

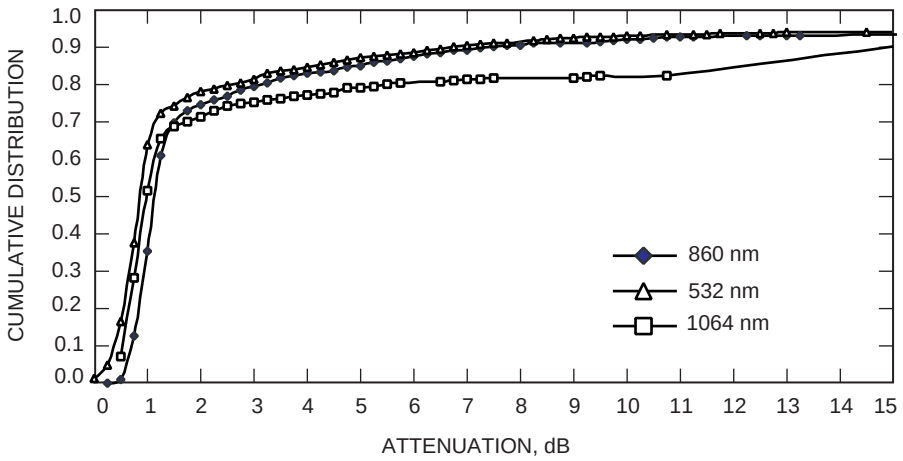

Fig. 6. The spectral transmission of the atmosphere represented by cumulative distribution functions for Alpha Bootis from January to April 2000.

for this. Consequently, the 1064-nm window is artificially weighted towards large dB attenuation. This preliminary plot does not account for weather outages, system outages, or instances when the camera exposures were at their minimum or maximum limits. Only 58 percent of the possible data was gathered, and only 67 percent of it was of the appropriate exposure and not otherwise corrupt. Further analysis is being performed on the data to clear up its representation. Although a more detailed comparison of these results with the older data acquired using the AVM is forthcoming, the data in Fig. 6 do show a resemblance to previously acquired data at TMF. One of the most remarkable features of the new data represented in Fig. 6 is that they include daytime and nighttime observations, whereas with the old system predominantly nighttime observations were used.

A variation of the calibration plots also can be made to provide a useful application that was not previously explored. One begins by plotting the measured star intensities, as a percentage of the maximum measured, against the elevation angle of the measurement. By considering the average of the 90 percent box of intensity values, a measure of attenuation versus elevation may be determined. This is of particular interest to nongeosynchronous laser-communication links, where the transmitted laser power may be varied as a function of elevation to maintain a constant link margin across the pass. A preliminary plot demonstrating this application is shown in Fig. 7.

III. Future Work

A number of modifications and improvements are underway for the AVM system, both in its range of data-acquisition capabilities and in the interpretation of its current data. These are discussed below.

(1) Sky polarization will be measured by removing the three astronomical filters (which currently are not being used for data analysis) and replacing them with 1064-nm filters coupled with thin-film polarization sheets oriented at three different angles with respect to the optical axis. By assuming that the polarization in the field of view remains relatively constant over the time it takes to take three images, one may use the results of these three images to determine the background polarization of the sky. This information is of particular interest as sky polarization may be used to limit the amount of background light that would be present in daytime observations, without severely altering the signal itself. Currently, all parts needed to implement this are being tested in the laboratory before implementation. After a trial period, a decision will be made as to whether or not to make this change permanent at all three sites.

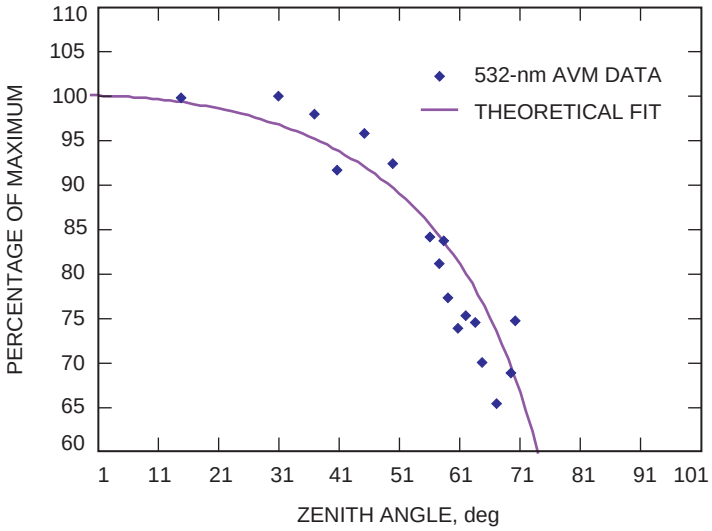

Fig. 7. Percent of maximum transmission as a function of zenith angle. Such a plot may be used to determine how to vary the power of a transmit laser as a satellite passes through different zenith angles to ensure that the power at the receiver remains constant. This plot was done at 532 nm, using the low-attenuation star images used for calibration. The theoretical fit was created using an attenuation value corresponding to about 18 percent at zenith.

(2) The National Climatic Data Center (NCDC) currently records human sky observations of the fraction of sky covered by clouds on a regular basis [9]. These observations are on a scale of one to eight. By comparing observed scales with AVM data, it may be possible to correlate dB losses with cloud cover. This has considerable consequences, because the NCDC locations are far more numerous than the number of AVM sites and are more broadly distributed. Thus, field-established optical communications theoretically could use current data to predict expected data-volume transmission statistics for many locations.

(3) Photometric observations can be performed with telescopes near both the Table Mountain AVM and the Mt. Lemmon AVM. These observations, when performed simultaneously with AVM observations, will permit a calculation of the throughput of the AVM, as well as verify the calibration values currently computed.

IV. Conclusion

The upgraded Atmospheric Visibility Monitor located at the Table Mountain Facility is producing valid data. Not enough data have been gathered at the Mt. Lemmon facility to assess the system's performance, but no indication of any further data-acquisition process error is apparent yet. The process for data analysis is being improved incrementally, and critical evaluation will continue to seek enhanced reliability. Reasonable cumulative distribution functions have been produced.

Acknowledgments

The authors would like to thank Keith Wilson for his review and comments. They also would like to acknowledge the invaluable assistance of Jon Depew, David Erickson, Jason Beebe, John Sandusky, and Muthu Jeganathan.

References

[1] A. Biswas and S. Lee, "Ground-to-Ground Optical Communications Demonstration," *The Telecommunications and Mission Operations Progress Report 42-141, January–March 2000*, Jet Propulsion Laboratory, Pasadena, California, pp. 1–31, May 15, 2000.
http://tmo.jpl.nasa.gov/tmo/progress_report/42-141/141G.pdf

[2] T.-Y. Yan, "Atmospheric Transmission Model Through Autonomous Visibility Measurement," *SPIE Proceeding*, vol. 2123, pp. 400–408, 1994.

[3] M. Jeganathan and D. Erickson, "An Overview of the Atmospheric Visibility Monitoring (AVM) Program," *SPIE Proceeding*, vol. 2990, pp. 114–120, 1997.

[4] M. Jeganathan and N. Jalali, "Analysis of Data From the Atmospheric Visibility Monitoring (AVM) Program," *SPIE Proceeding*, vol. 3266, pp. 200–208, 1998.

[5] H. Hemmati, K. Wilson, M. K. Sue, L. J. Harcke, M. Wilhelm, C.-C. Chen, J. R. Lesh, Y. Feria, D. Rascoe, F. Lansing, and J. W. Layland, "Comparative Study of Optical and Radio-Frequency Communications Systems for a Deep-Space Mission," *The Telecommunications and Data Acquisition Progress Report 42-128, October–December 1996*, Jet Propulsion Laboratory, Pasadena, California, pp. 1–33, February 15, 1997.
http://tmo.jpl.nasa.gov/tmo/progress_report/42-128/128N.pdf

[6] D. Erickson, D. H. Tsiang, and M. Jeganathan, "Upgrade of the Atmospheric Visibility Monitoring system," *SPIE Proceeding*, vol. 3615, pp. 310–315, 1999.

[7] V. E. Zuev, "Laser-Light Transmission Through the Atmosphere," in *Topics in Applied Physics*, vol. 14, *Laser Monitoring of the Atmosphere*, E. D. Hinkley, editor, New York: Springer-Verlag, pp. 29–67, 1976.

[8] R. F. Calfee, "Infrared Absorption Properties of Atmospheric Gases," *J. Quant. Spectr. Rad. Transfer*, vol. 6, p. 221, 1966.

[9] V. E. Zuev, M. V. Kabanov, and B. A. Savelev, "Propagation of Laser Beams in Scattering Media," *Appl. Opt.*, vol. 8., p. 137, 1969.

Appendix

Process Flow of the Flagging Routine

Figure A-1 provides the process flow of the flagging routine to be implemented as a part of the on-site image processing.

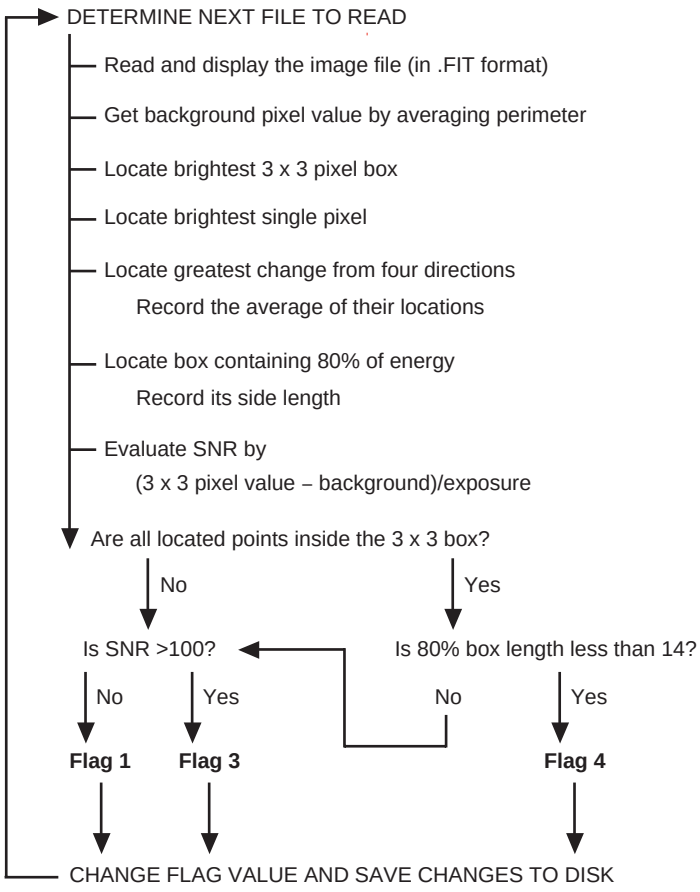

Fig. A-1. Process flow of the flagging routine.